Catalysis Letters
https://doi.org/10.1007/s10562-019-02719-5

Facile Synthesis of CuO–Ni/Al Composites for Catalytic Oxidation of Cyclohexene

Ang Ma[1] · **YangYang Cheng**[1] · **Yijia Bai**[1,2] · **Jianmin Hao**[1,2] · **Fumin Chu**[1] · **Limin Han**[1,2] · **Huacong Zhou**[1,2]

Received: 10 September 2018 / Accepted: 19 February 2019
© Springer Science+Business Media, LLC, part of Springer Nature 2019

Abstract

CuO–Ni/Al composites were synthesized by electroless deposition and thermal oxidation and characterized by inductively coupled plasma optical emission spectrometry, X-ray powder diffraction, scanning electron microscopy and X-ray photoelectron spectroscopy. Their performances as the heterogeneous catalysts for the solvent-free allylic oxidation of cyclohexene by oxygen were determined. It was found that the CuO contents and the amount of adsorbed oxygen species on the composites could significantly affect their catalytic performances in cyclohexene oxidation. The highest catalytic activity was achieved over CuO–Ni/Al-3 containing 18.5 wt% CuO with the highest amount of adsorbed oxygen species, which resulted in the maximum cyclohexene conversion of 39.1% and the total selectivity of 85.5% to 2-cyclohexene-1-ol, 2-cyclohexene-1-one, 2-cyclohexene-1-hydroperoxide and cyclohexene oxide. In addition, the catalyst was successfully recycled with no significant catalytic activity loss after three cycles.

Graphical Abstract

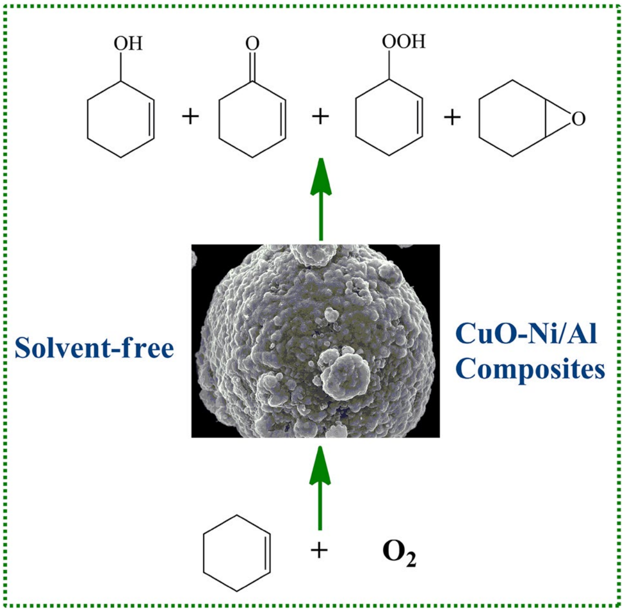

Keywords Electroless deposition · Thermal oxidation · Cyclohexene oxidation · Heterogeneous catalysis · Oxygen

---

Electronic supplementary material The online version of this article (https://doi.org/10.1007/s10562-019-02719-5) contains supplementary material, which is available to authorized users.

Extended author information available on the last page of the article

Published online: 28 February 2019

1 Introduction

Copper oxide (CuO), an attractive metal oxide, has been extensively applied in photoelectron chemistry, solar cell, electrochemistry and catalysis [1–4]. It can be simply prepared by the thermal oxidation of Cu at less cost [5–7]. For a typical preparation process, Cu metallization is often the first step. It can be achieved by electroless deposition, which produces a Cu deposit on the support surface via the reduction of copper ions with a reducing agent in solution [8]. Such metallization is a catalytic/autocatalytic redox process requiring catalytic active sites on the support surface that are usually from the support material itself or achieved via modifications with catalytically active metals [9, 10]. The metalized Cu is then further oxidized to form CuO. It has been reported that the CuO nanoparticles supported on silicon nanowires prepared by the electroless deposition and thermal oxidation exhibited excellent performances in detecting nonenzymatic H_2O_2 with the detection limit as low as 1.6 μM [11]. The CuO/Co/carbon fiber (CF) composites prepared by electroless deposition and annealing at 673 K in air was found with strong magnetic loss and microwave adsorption [12]. So the electroless deposition and thermal oxidation could be used to synthesize CuO composites conveniently and effectively.

The allylic oxidation of cyclohexene can produce value-added products, such as 2-cyclohexene-1-ol (Cy-ol), 2-cyclohexene-1-one (Cy-one) and 2-cyclohexene-1-hydroperoxide (Cy-HP), and thus has attracted considerable attentions in both academic study and industrial production [13]. Green and sustainable catalytic oxidation processes, such as solvent-free oxidation by O_2, has been promoted for environmental protection. Such catalytic oxidations are usually conducted with heterogeneous catalysts due to the advantages of high stability, easy separation and reutilization. For example, Zou et al. achieved 25.4% cyclohexene conversion with 96.6% total selectivity to Cy-ol and Cy-one over the hollow framework TS-1 (MTS-1) containing 5 wt% manganese at 343 K using 0.4 MPa O_2 without no solvent required [14]. CuO nanoleaves with both mesoporous structure and nanostructure were found with excellent catalytic activity for the solvent-free oxidation of cyclohexene at 353 K under 1 atm O_2 [15].

We reported previously the excellent catalytic performance of CuNi-ELD/Co composite containing 6.0 wt% amorphous Cu in the solvent-free oxidation of cyclohexene by O_2 [16]. However, the weak adhesive force between the Cu deposit and Co powder caused the falling-off of Cu deposit in the recycled catalyst, even after one cycle, which was unconducive to the catalyst recycle. Meanwhile, we found that Al powder could also provide special surface species as the nucleation sites of Cu crystallization with no traditional treatments for the sensitization–activation of $SnCl_2$–$PdCl_2$ required during electroless Cu deposition. In addition, thermal oxidation may be able to strengthen the adhesive force between the deposit and matrix metal. Herein, CuO–Ni/Al composites were prepared by electroless deposition and thermal oxidation under different conditions and characterized by ICP-OES, XRD, SEM and XPS. Their application as the heterogeneous catalyst for the solvent-free allylic oxidation of cyclohexene by O_2 was explored. The optimal composite catalyst was successfully recycled with slightly decreased catalytic activity.

2 Experimental

2.1 Synthesis of CuO–Ni/Al Composites

Certain amounts of $CuSO_4·5H_2O$ (0.6 g, AR), $Na_3C_6H_5O_7·2H_2O$ (2 g, AR), 2,2′-bipyridine (1 mg, AR), $CH_3(CH_2)_{11}OSO_3Na$ (0.4 mg, AR), $NiSO_4·6H_2O$ (0.05 g, AR) and $NaH_2PO_2·H_2O$ (3.8 g, AR) were added into a round-bottomed flask containing 100 mL deionized water, and stirred until completely dissolved. The pH of the solution was adjusted to ~ 8.5 with NaOH. A certain amount of Al powder (20 μm, ≥ 99%) pre-coarsened in HF solution was added to the plating solution at the desired molar ratio between Al and Cu and stirred constantly for 2.5 h at 333 K. The color of the solid particles gradually changed from silvery white (Al) to red (Cu). The particles were then collected by filteration, washed by deionized water, dried at 323 K for 4 h in air, milled, sintered in a muffle furnace at 773 K for 6 h and milled again to afford CuO–Ni/Al composites. Other catalysts were prepared as described in the supplementary material.

2.2 Characterization

The metal contents in the prepared CuO–Ni/Al composites were determined with a Thermo Fisher Scientific ICAP 6300 inductively-coupled plasma optical emission spectrometer. XRD spectra were recorded on a Bruker D8 Advance X-ray powder diffractometer using Cu Kα in the range of 10°–90°. The surface morphologies were imaged with a Hitachi S-3400N scanning electron microscope. The electronic properties of surface elements were analyzed with a Thermo Escalab 250Xi X-ray photoelectron spectroscope. The binding energies were referenced to the C 1s line of adventitious carbon at 284.8 eV. The Brunauer–Emmett–Teller (BET) specific surface areas of the composites were measured using a Quantachrome Quadrasorb SI-KR/MP gas sorption surface area and pore size analyzer.

2.3 Catalytic Tests

The catalytic cyclohexene oxidation was conducted in a magnetically stirred 50-mL PTFE-lined autoclave. Briefly, 5 mL cyclohexene and a certain amount of CuO–Ni/Al composite were added into the reactor, heated at 351 K in 2 MPa O_2 atmosphere in an oil bath for 6 h under constant stirring and cooled in an ice-bath for 1 h. The residual gas was released slowly and the reaction solution was filtered. The filtrate was analyzed qualitatively by GC–MS and quantitatively analyzed using a SHIMADZU GC-14C quipped with a RTX-50 column. The GC column temperature was programmed as: initial temperature 313 K, held for 5 min, increased to 493 K at the heating rate of 10 K/min, and held for 5 min. The conversion and selectivity were calculated by the area normalization method using the relative correction factors as follows:

$$Conversion\,(\%) = \left(1 - \frac{A_c f_c}{A_c f_c + A_1 f_1 + A_2 f_2 + A_3 f_3 + \cdots A_i f_i}\right) \times 100\%$$

$$Selectivity\,(\%) = \left(\frac{A_i f_i}{A_1 f_1 + A_2 f_2 + A_3 f_3 + \cdots A_i f_i}\right) \times 100\%$$

where A_c is the GC peak area of residual cyclohexene, f_c is the relative correction factor of cyclohexene, A_i is the GC peak area of product *i*, f_c is the relative correction factor of product *i*. The relative correction factor was calculated based on the difference between the substance amounts with the same GC peak area.

3 Results and Discussion

3.1 Characterization of CuO–Ni/Al Composites

A certain amount of CuO–Ni/Al was dissolved in HNO_3–HCl and analyzed by ICP-OES for metal contents as shown in Table 1. The theoretical mole ratio of Cu/Al in the composite ranged from 1:30 to 1:5 with a fixed Ni/Cu mole ratio of 1:12.6. The experimental Al contents were lower than the corresponding theoretical values because partial Al reacted with OH^- to form AlO_2^-, and thus was leached from Al powder in the alkaline solution during electroless Cu deposition. However, no $Cu(OH)_2$ was formed due to the complexation of Cu ions with sodium citrate. Ni^{2+} acted as the catalyst for hypophosphite oxidation to enable the continuous deposition of Cu, resulting in the co-deposited of Ni and Cu (Fig. S1) [17, 18]. Higher Ni^{2+} concentrations can accelerate the Cu deposition. However, extremely high deposition rates are unconducive to the formation of a smooth Cu deposit coating. The optimal Ni^{2+}/Cu^{2+} mole ratio was determined to be 1:12.6. The experimental Ni^{2+}/Cu^{2+} mole ratios of CuO–Ni/Al-1 and CuO–Ni/Al-2 are higher than the corresponding theoretical values, indicating the incomplete reduction of Cu^{2+} in these composites. When increasing the Cu/Al mole ratios, the amount of Cu deposit per unit surface area of Al powder increased with the decrease of the amount of Al powder, resulting in the decrease of the experimental Ni^{2+}/Cu^{2+} mole ratios.

Figure 1 shows the XRD patterns of CuO–Ni/Al composites prepared under different conditions. Pure Al powder exhibited five strong peaks at $2\theta = 38.7°$, 44.9°, 65.3°, 78.4° and 82.8°, which were respectively ascribed to the

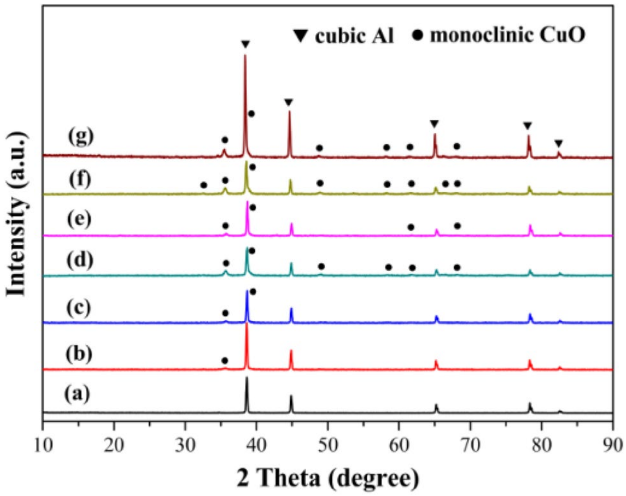

Fig. 1 XRD patterns of pure Al powder (a), CuO–Ni/Al-1 (b), CuO–Ni/Al-2 (c), CuO–Ni/Al-3 (d), CuO–Ni/Al-4 (e), CuO–Ni/Al-5 (f) and CuO–Ni/Al-3 recycled after one cyclohexene oxidation cycle (g)

Table 1 Chemical compositions of CuO–Ni/Al composites

Entry	Sample	n_{Cu}/n_{Al} theoretical	n_{Cu}/n_{Al} actual	n_{Ni}/n_{Cu} theoretical	n_{Ni}/n_{Cu} actual	wt%		
						CuO	Al	Ni
1	CuO–Ni/Al-1	1:30	1:24	1:12.6	1:7	10.8	88.1	1.1
2	CuO–Ni/Al-2	1:20	1:18.5	1:12.6	1:7.7	13.6	85.1	1.3
3	CuO–Ni/Al-3	1:15	1:12.8	1:12.6	1:13.5	18.5	80.5	1.0
4	CuO–Ni/Al-4	1:10	1:8.4	1:12.6	1:19.1	25.7	73.3	1.0
5	CuO–Ni/Al-5	1:5	1:2.9	1:12.6	1:25.5	49.7	48.9	1.4

(111), (200), (220), (311) and (222) planes of cubic Al phase (JCPDS, No. 04-0787) (Fig. 1a). The thermal oxidation did not change the cubic Al phase in the composites significantly and no aluminum oxide was detected. The 2θ peak of CuO–Ni/Al-1 with a low Cu content at 35.5° was indexed to the preferred orientation (11-1) plane of monoclinic CuO phase (JCPDS, No. 48-1548) (Fig. 1b). Increasing the Cu content resulted in more diffraction peaks at $2\theta = 32.5°$, 38.7°, 48.7°, 58.2°, 61.5°, 66.2° and 68.1° that were assigned to the (110), (111), (20-2), (202), (11-3), (31-1) and (220) planes of monoclinic CuO phase, respectively (Fig. 1c–f). The weak and broad diffraction peaks of the monoclinic CuO phase in the composites indicate their low crystallinity due to more crystal defects and poor crystal growth quality caused by the Ni atoms doped in the Cu lattice [19]. The characteristic XRD diffraction peaks of cubic Al and monoclinic CuO of CuO–Ni/Al-3 remained unchanged after one reaction cycle, indicating that the integrate structure of the composite was maintained during the oxidation.

Figure 2 shows the XPS spectra of CuO–Ni/Al composites prepared under different conditions. All composites exhibited the Cu 2p$_{3/2}$ and Cu 2p$_{1/2}$ peaks at 933.8 eV and 953.7 eV, respectively, with the doublet separation of 19.9 eV, and satellite features at 943 eV and 962.5 eV of CuO. The peaks of pure Al powders at 71.9 eV and 74.4 eV were respectively attributed to the metallic Al and oxidized Al, suggesting that the Al particle surface was partially covered with a passive Al_2O_3 film. The Al-ELD powders that was treated with the same electroless deposition process, but in the absence of $CuSO_4{\cdot}5H_2O$, exhibited the characteristic XPS peaks of AlOOH or $Al(OH)_3$. The aluminum hydroxide(s) was completely oxidized to Al_2O_3 during the thermal oxidation, affording Al-ELD-TO powder. Both CuO and Al_2O_3 phases were found in all CuO–Ni/Al composites with overlapped Cu 3p and Al 2p peaks that were resolved to be at 78.4 eV and 75.8 eV, respectively [20, 21]. The detailed peak fitting results for the relative atomic ratios of Cu and Al are shown in Table 2. The highest surface Cu content was found on CuO–Ni/Al-3. The O 1s spectra of pure Al powder, Al-ELD powder and Al-ELD-TO powder suggested the presence of aluminum oxide. The O 1s curves of all CuO–Ni/Al composites were deconvoluted into three peaks at ~529.8 eV, ~531.7 eV and ~533.1 eV, respectively, that were denoted as $O_{I,}$ O_{II} and O_{III}. The O_I and O_{II} peaks were attributed to Cu–O and Al–O, respectively [22]. The introduction of CuO shifted the Al 2p peak to the high bonding energy region and O 1s peak to the low bonding energy region, because Cu with a higher electronegativity enhanced the polarization of Al–O [23]. The O_{III} peak was due to the adsorbed and dissociated surface oxygen species, such as $O_{2,}$ O_2^- and O^-, which were formed during the thermal oxidation in the oxidizing atmosphere [24]. It has been reported that the oxygen adsorption and vacancy coexist and interact

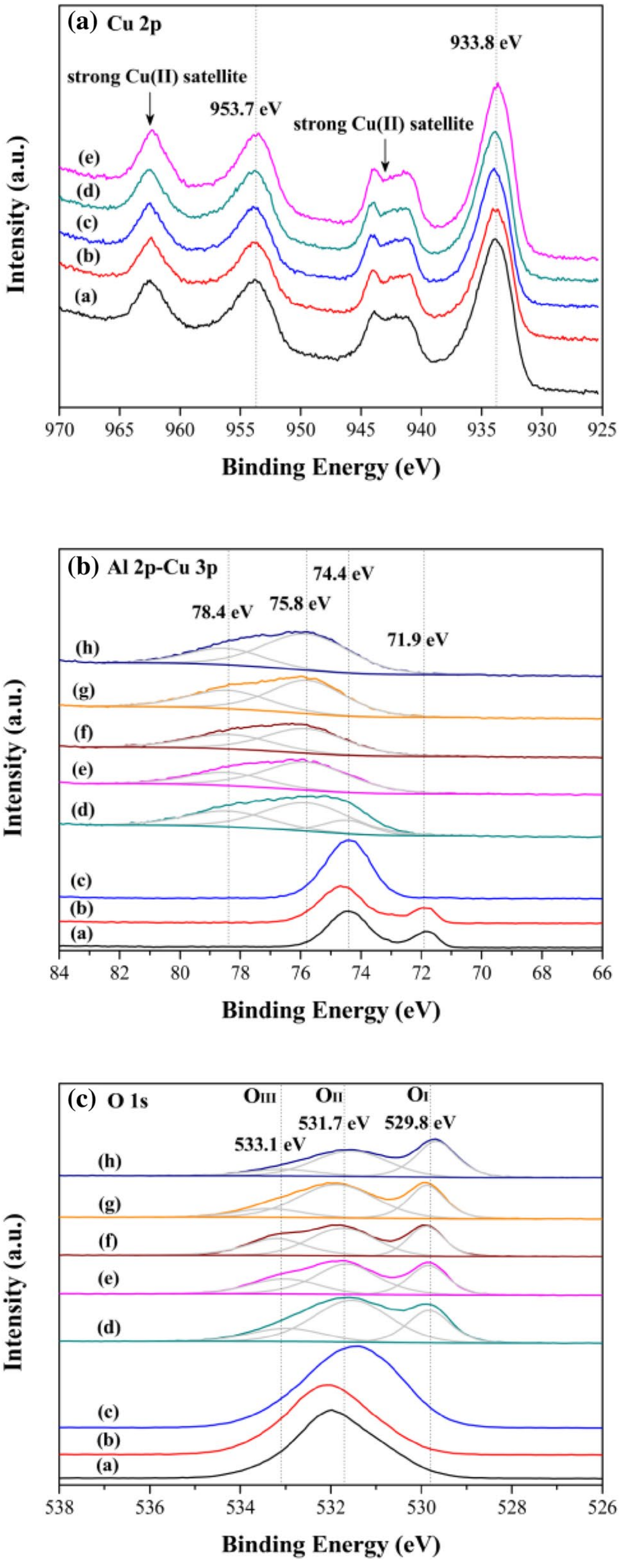

Fig. 2 **a** Cu 2p XPS spectra of CuO–Ni/Al-1 (a), CuO–Ni/Al-2 (b), CuO–Ni/Al-3 (c), CuO–Ni/Al-4 (d) and CuO–Ni/Al-5 (e); **b** Al 2p-Cu 3p XPS spectra of pure Al powder (a), Al-ELD powder (b), Al-ELD-TO powder (c), CuO–Ni/Al-1 (d), CuO–Ni/Al-2 (e), CuO–Ni/Al-3 (f), CuO–Ni/Al-4 (g) and CuO–Ni/Al-5 (h); **c** O 1s XPS spectra of pure Al powder (a), Al-ELD powder (b), Al-ELD-TO powder (c), CuO–Ni/Al-1 (d), CuO–Ni/Al-2 (e), CuO–Ni/Al-3 (f), CuO–Ni/Al-4 (g) and CuO–Ni/Al-5 (h)

Table 2 Peak fitting results of the Al 2p-Cu 3p and O 1s XPS spectra for CuO–Ni/Al composites

CuO–Ni/Al composites	Al 2p-Cu 3p				O 1s					
	Al 2p		Cu 3p		O_I		O_{II}		O_{III}	
	B.E. (eV)	Area%	B.E. (eV)	Area%	B.E. (eV)	Area%	B.E. (eV)	Area%	B.E. (eV)	Area%
CuO–Ni/Al-1	75.8/74.5	72.5	78.4	27.5	529.8	25.3	531.5	57.5	533.0	17.2
CuO–Ni/Al-2	75.8	70.4	78.5	29.6	529.8	28.1	531.7	47.6	533.0	24.3
CuO–Ni/Al-3	75.8	61.7	78.3	38.3	529.9	28.2	531.7	46.9	533.1	24.9
CuO–Ni/Al-4	75.8	63.3	78.4	36.7	529.9	28.6	531.9	58.5	533.4	12.9
CuO–Ni/Al-5	75.8	71.4	78.5	28.6	529.7	39.9	531.6	48.1	533.1	12.0

with each other in p-type CuO, specifically, the adsorbed oxygen increases the oxidation states of Cu, which provides more oxygen vacancies to induce stronger oxygen adsorption at high temperatures in the oxidizing atmosphere [25, 26]. Importantly, the surface oxygen species and oxygen vacancies can be reactively involved in the oxidation process and contribute to the high catalytic activity significantly [27, 28]. The relative proportions of $O_{I,}$ O_{II} and O_{III} peak areas listed in Table 2 suggest that CuO–Ni/Al-3 surface possessed the highest amount of adsorbed oxygen species. The high amount of surface oxygen species can improve the redox properties of the composite, and is thus conducive to the catalytic oxidation of cyclohexene.

The surface morphologies of CuO–Ni/Al composites were imaged by SEM. The Al particles in CuO–Ni/Al-1 with a low Cu content were partially coated with the CuO deposit (Fig. 3a). For CuO–Ni/Al-2 with a higher Cu content, the surface coverage of Al particles with CuO deposit was increased and the CuO crystals agglomerated into different sizes of aggregates, indicating a CuO coating layer was almost formed (Fig. 3b). The CuO deposit became tight and smooth on the surface of CuO–Ni/Al-3 with a few pores that provided contact sites between CuO and Al_2O_3 (Fig. 3c). As the Cu content further increased, Al particles were completely coated with a CuO film, and the CuO coating layer became rough and loose due to more CuO crystalline grains of different morphologies and sizes formed on the surface (Fig. 3d, e).

3.2 Catalytic Oxidation of Cyclohexene Over CuO–Ni/Al Composites by Oxygen

The catalytic activities of CuO–Ni/Al composites for the oxidation of cyclohexene by oxygen were then evaluated. The reaction mainly produced Cy-ol, Cy-one, Cy-HP and cyclohexene oxide (Cy-oxide) (Fig. 4) as identified by GC–MS (Fig. S2). The potential reaction pathways were also presumed for the catalytic oxidation of cyclohexene over CuO–Ni/Al composites by oxygen according to the literature [29, 30] (Fig. S3). It subjects to a typical radical-chain reaction mechanism. At beginning the homolytic cleavage of the α-C–H bond of cyclohexene produces allylic cyclohexenyl radical, which reacts with O_2 to form the dominant radical species cyclohexenyl peroxyl radical (Cy-OO·). The generated Cy-HP behaves as the principal source of main products. It directly decomposes to Cy-one and Cy-ol or to Cy-one and water in the presence of CuO–Ni/Al composites through redox cycling between Cu(II) and Cu(I) oxidation states. It is also converted to Cy-ol and Cy-oxide through the epoxidation of cyclohexene, and Cy-oxide is hydrolyzed to 1,2-cyclohexanediol.

The cyclohexene conversion was only 7.9% in the absence of catalyst (Table 3 entry 1), and was only increased to 11.1% over pure Al powder catalyst (Table 3 entry 2), similar to those over Al-ELD and Al-ELD-TO catalysts (Table 3 entries 3 and 4), suggesting the low catalytic activities of these catalyst supports. The cyclohexene conversion was further slightly increased to 13.8% and 15.1% over CuO–Ni/Al-1 and CuO–Ni/Al-2 with low CuO contents, respectively (Table 3 entries 5 and 6). CuO–Ni/Al-3 catalyst containing 18.5 wt% CuO gave the highest cyclohexene conversion of 39.1% (Table 3 entry 7). Further increasing the CuO contents resulted in lower conversions of cyclohexene (Table 3 entries 8 and 9). These results indicate that the CuO–Ni deposit on the CuO–Ni/Al is the active catalytic species and the CuO content affects its catalytic activity evidently. The appropriate CuO content in CuO–Ni/Al composite can provide the maximum dispersion of CuO–Ni species and the higher amount of adsorbed oxygen species on Al support, and more CuO content cannot further improve the dispersion of CuO–Ni species because of the high crystallinity.

To further investigate the role of Ni in the catalytic activity of CuO–Ni/Al composite, Ni/Al-3-TO composite was synthesized at the Ni/Al mole ratio of 1:15, same as that in CuO–Ni/Al-3. The cyclohexene conversion over Ni/Al-3-TO was found to be 12.2% (Table 3 entry 10), similar to that over the catalyst supporter. CuO/Al-3 with no Ni species prepared by formaldehyde reducing agent resulted in the cyclohexene conversion of 34.3% (Table 3 entry

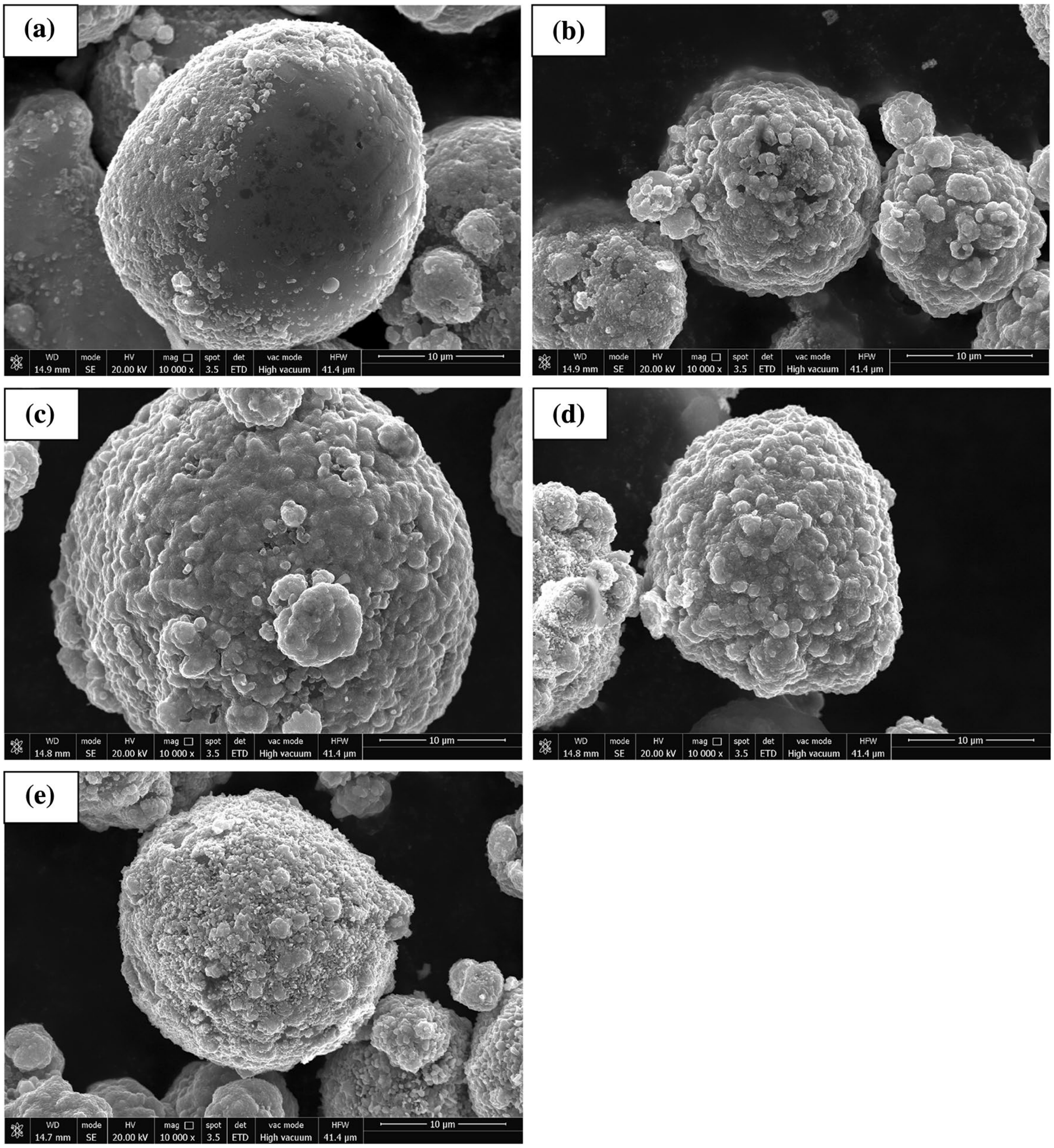

Fig. 3 SEM images of CuO–Ni/Al-1 (**a**), CuO–Ni/Al-2 (**b**), CuO–Ni/Al-3 (**c**), CuO–Ni/Al-4 (**d**) and CuO–Ni/Al-5 (**e**)

Fig. 4 Catalytic oxidation of cyclohexene over CuO–Ni/Al composites by oxygen

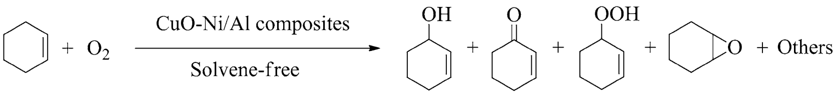

11), lower than that over CuO–Ni/Al-3. These results indicate the Ni deposit alone has no catalytic activity, but can promote the catalytic activity of CuO–Ni/Al composite. And hypophosphite was used as the reducing agent for the electroless Cu deposition, which made the process more environmentally benign, as compared with conventional methods using formaldehyde as the reducing agent.

The cyclohexene conversion over the mixture of CuO and Al-ELD-TO powder was determined to be 22.0% (Table 3 entry 12), much lower than that over CuO–Ni/Al-3 catalyst.

Table 3 Catalytic performance of different catalysts in the oxidation of cyclohexene

Entry	Catalyst	Conv. (%)	Selectivity (%)				
			Cy-ol	Cy-one	Cy-HP	Cy-oxide	Others
1	–	7.9	13.2	59.1	24.9	1.1	1.7
2	Pure Al powder	11.1	6.7	22.7	64.8	2.2	3.6
3	Al-ELD powder	10.9	6.2	69.5	20.7	2.2	1.4
4	Al-ELD-TO powder	11.9	14.8	39.0	35.8	2.0	8.4
5	CuO–Ni/Al-1	13.8	9.2	28.2	54.2	3.1	5.3
6	CuO–Ni/Al-2	15.1	9.6	27.5	51.3	2.1	9.5
7	CuO–Ni/Al-3	39.1	10.4	31.8	41.0	2.3	14.5
8	CuO–Ni/Al-4	29.2	10.4	32.3	41.2	5.3	10.8
9	CuO–Ni/Al-5	16.7	18.1	41.2	32.0	1.3	7.4
10	Ni/Al-3-TO	12.2	9.3	28.4	58.4	2.7	1.2
11	CuO/Al-3	34.3	9.7	29.8	45.1	3.1	12.3
12	CuO + Al-ELD-TO powder	22.0	10.7	32.5	38.3	2.5	16.0
13	CuO–Ni/Al_2O_3-3	25.9	11.9	23.1	50.6	4.2	10.2
14	Cu-Ni/Al-3	31.9	7.2	23.1	59.7	5.1	4.9
15	Cu-Ni/Al-3^{2nd}	24.9	7.9	26.5	55.8	3.3	6.5

Reaction conditions: cyclohexene 5 mL, O_2 2 MPa, reaction temperature 351 K, reaction time 6 h, mole ratio of Cu to cyclohexene 1:200

In addition, CuO–Ni/Al_2O_3-3 with the Cu/Al mole ratio of 1:15, where Al_2O_3 instead of Al was used as catalyst support, also resulted in a lower conversion of 25.9% (Table 3 entry 13), as compared with that over CuO–Ni/Al-3. These results indicate that the Al support matrix and CuO deposit exhibited a synergistic effect on the catalytic activity. The Al support matrix provided free electrons to accelerate the conversion of the adsorbed oxygen species to active oxygen species, which enhanced the abstraction of the weakly bonded allylic hydrogen atom of cyclohexene to form cyclohexenyl peroxyl radical (Cy-OO$^{\cdot}$), the dominant radical species in cyclohexene oxidation radical-chain reaction [16, 29, 30]. Therefore, CuO–Ni/Al-3 composite was able to provide more active CuO sites and a higher amount of adsorbed oxygen species according to XPS results, and thus exhibited the excellent catalytic performance in cyclohexene oxidation.

The cyclohexene conversion over Cu-Ni/Al-3 composite prepared by electroless deposition was 31.9% (Table 3 entry 14), slightly lower than that over CuO–Ni/Al-3, but was significantly decreased to 24.9% in the second oxidation cycle (Table 3 entry 15), possibly due to the falling-off of Cu deposit from the composite (Fig. S4). In contrast, the cyclohexene conversion over CuO–Ni/Al-3 was only slightly decreased after three cycles (Fig. 5), suggesting that the thermal oxidation strengthened the adhesion and interaction between the CuO–Ni deposit and Al support. In addition, no metal loss was found in the product solution after the reaction, indicating that the oxidation occurred on the CuO–Ni/Al-3 catalyst surface heterogeneously.

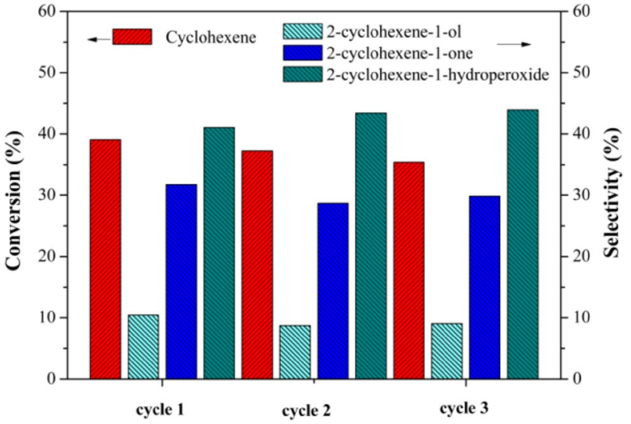

Fig. 5 Recycle of CuO–Ni/Al-3 catalyst. Reaction conditions: cyclohexene 5 mL, O_2 2 MPa, reaction temperature 351 K, reaction time 6 h, mole ratio of Cu to cyclohexene 1:200

4 Conclusions

In summary, CuO–Ni/Al composites containing cubic Al and monoclinic CuO phases were synthesized by electroless deposition and thermal oxidation, and their application as a heterogeneous catalyst for the solvent-free allylic oxidation of cyclohexene by oxygen was explored. The results suggest that their catalytic performance was strongly dependent on the CuO content and the amount of adsorbed oxygen species. In addition, the Ni species also contributed to the high catalytic activity of the composite and the Al support exhibited a synergistic effect with CuO deposit on the catalytic performance of the composite in the oxidation of cyclohexene. Among all prepared composites, CuO–Ni/Al-3 containing 18.5 wt% CuO exhibited the highest catalytic activity and the highest amount of adsorbed oxygen species. In addition, it was successfully recycled with no significant catalytic activity losses after three cycles due to the strong adhesion and interaction between the CuO–Ni deposit and Al support achieved by thermal oxidation.

Acknowledgements This work was financially supported by the National Natural Science Foundation of China (No. 21163011), the Natural Science Foundation of Inner Mongolia (Grant No. 2017MS(LH)0205) and the Research Program of Science and Technology at Universities of Inner Mongolia Autonomous Region (Grant No. NJZZ17081).

Compliance with Ethical Standards

Conflict of interest The authors declare no conflict of interest.

References

1. Lim YF, Chua CS, Lee CJJ et al (2014) Phys Chem Chem Phys 16:25928
2. Sharma JK, Akhtar MS, Ameen S et al (2015) J Alloys Compd 632:321
3. Chen LB, Lu N, Xu CM et al (2009) Electrochim Acta 54:4198
4. Jammi S, Sakthivel S, Rout L et al (2009) J Org Chem 74:1971
5. Jiang X, Herricks T, Xia Y (2002) Nano Lett 2:1333
6. Horak P, Bejsovec V, Vacik J et al (2016) Appl Surf Sci 389:751
7. Li J, Zhang Z, Ji Y et al (2016) Nano Res 9(5):1377
8. Nobari N, Behboudnia M, Maleki R (2016) Appl Surf Sci 385:9
9. Reddy EL, Lee HC, Kim DH (2015) Int J Hydrogen Energy 40:2509
10. Naruškevičius L, Tamašauskaitė-Tamašiūnaitė L, Žielienė A et al (2012) Surf Coat Technol 206:2967
11. Huang J, Zhu Y, Zhong H et al (2014) ACS Appl Mater Interfaces 6:7055
12. Zeng J, Fan H, Wang Y et al (2012) Thin Solid Films 520:5053
13. Godhani DR, Nakum HD, Parmar DK et al (2016) J Mol Catal A 415:37
14. Zou G, Jing D, Zhong W et al (2016) RSC Adv 6:3729
15. Sang X, Zhang J, Wu T et al (2015) RSC Adv 5:67168
16. Hao J, Jiao X, Han L et al (2015) RSC Adv 5:13809
17. Cheng DH, Xu WY, Zhang ZY et al (1997) Met Finish 95:34
18. Gan X, Wu Y, Liu L et al (2007) Surf Coat Technol 201:7018
19. Li J, Hayden H, Kohl PA (2004) Electrochim Acta 49:1789
20. Figueiredo RT, Martínez-Arias A, Granados ML et al (1998) J Catal 178:146
21. Li F, Zhang L, Evans DG et al (2004) Colloids Surf A 244:169
22. Kim KM, Kwak BS, Park NK et al (2017) J Ind Eng Chem 46:324
23. Igbari O, Xie Y, Jin Z et al (2015) J Alloys Compd 653:219
24. Wang Y, Lü Y, Zhan W et al (2015) J Mater Chem A 3:12796
25. Sun S, Li C, Zhang D et al (2015) Appl Surf Sci 333:229
26. Zhong K, Xue J, Mao Y et al (2012) RSC Adv 2:11520
27. Menon U, Galvita VV, Marin GB (2011) J Catal 283:1
28. Rao BG, Sudarsanam P, Nallappareddy PRG et al (2017) Catal Commun 101:57
29. Panov GI, Dubkov KA, Starokon EV (2006) Catal Today 117:148
30. Zhang R, Tang R (2016) J Mater Sci 51:5802

Publisher's Note Springer Nature remains neutral with regard to jurisdictional claims in published maps and institutional affiliations.

Affiliations

Ang Ma[1] · **YangYang Cheng**[1] · **Yijia Bai**[1,2] · **Jianmin Hao**[1,2] · **Fumin Chu**[1] · **Limin Han**[1,2] · **Huacong Zhou**[1,2]

✉ Jianmin Hao
haojmin@foxmail.com

[1] College of Chemical Engineering, Inner Mongolia University of Technology, Hohhot 010051, China

[2] Inner Mongolia Engineering Research Center for CO2 Capture and Utilization, Hohhot 010051, China